

Article

Rockfall Mapping and Monitoring Across the Kalymnos Sport Rock Climbing Sites, Based on Ultra-High-Resolution Remote Sensing Data and Integrated Simulations

Emmanuel Vassilakis ^{1,*} , Aliko Konsolaki ¹ , Konstantinos Soukis ¹ , Sofia Laskari ¹ , Evelina Kotsi ¹ ,
John Lialiaris ² and Efthymios Lekkas ¹

¹ Department of Geology and Geoenvironment, School of Science, National and Kapodistrian University of Athens, 15784 Athens, Greece; alikikons@geol.uoa.gr (A.K.); soukis@geol.uoa.gr (K.S.); slaskari@geol.uoa.gr (S.L.); ekotsi@geol.uoa.gr (E.K.); elekkas@geol.uoa.gr (E.L.)

² Geodesign PPC, 12134 Peristeri, Greece; lialiarisj@gmail.com

* Correspondence: evasilak@geol.uoa.gr; Tel.: +30-210-727-4400

Abstract: This manuscript presents a multidisciplinary study that proposes a methodology for delineating and categorizing vulnerability at rockfall risk areas to avoid human injuries and infrastructure damage caused by rockfalls. The presented workflow includes (i) classical geological mapping, (ii) the interpretation of high-resolution satellite data for observing the spatial distribution of fallen boulders, (iii) analytical hierarchy processing of spatial information within a Geographical Information System (GIS) platform, (iv) close-range remote sensing campaigns with Unmanned Aerial Systems (UASs), and (v) integrated simulation of rockfall events. This methodology was applied to Kalymnos Island, which belongs to the Dodecanese Islands complex of the southeastern Aegean Sea in Greece. It is characterized by unique geomorphological features, including extensive vertical limestone cliffs that span the island. These cliffs make it one of the world's most densely concentrated areas for sport climbing. The results highlighted the areas that the local authorities need to focus on and suggested measures for increasing the safety of climbers and infrastructure.

Keywords: Unmanned Aerial Systems; Structure-from-Motion; WorldView-3; analytical hierarchy processing; GIS



Citation: Vassilakis, E.; Konsolaki, A.; Soukis, K.; Laskari, S.; Kotsi, E.; Lialiaris, J.; Lekkas, E. Rockfall Mapping and Monitoring Across the Kalymnos Sport Rock Climbing Sites, Based on Ultra-High-Resolution Remote Sensing Data and Integrated Simulations. *Land* **2024**, *13*, 1873. <https://doi.org/10.3390/land13111873>

Academic Editor: Karel Charvat

Received: 16 August 2024

Revised: 2 November 2024

Accepted: 5 November 2024

Published: 9 November 2024



Copyright: © 2024 by the authors. Licensee MDPI, Basel, Switzerland. This article is an open access article distributed under the terms and conditions of the Creative Commons Attribution (CC BY) license (<https://creativecommons.org/licenses/by/4.0/>).

1. Introduction

Sport rock climbing has become more popular during the last few decades, and natural climbing sites are often located at geosites, which are areas of significant geological interest [1]. These geosites, when they include massive rocks with vertical slopes that are ideal for climbing, hold great potential to attract climbers along with other geotourists, thereby boosting the local economy. The incomparable natural beauty of Kalymnos Island and its geomorphological uniqueness makes it a destination for thousands of tourists and climbers worldwide, every year. However, the geomorphological characteristics of these areas make them highly susceptible to rockfalls, and the presence of people in these environments significantly increases the associated risks to extremely high levels. Although Kalymnos is a relatively small island, covering just 111 square kilometers, it is a place where over 4000 sport climbing routes have been marked. This vast number makes it challenging to study each site individually, highlighting the need for a generalized spatial analysis to prioritize the sites requiring further attention.

Rockfalls, as one of the most frequent and insidious landslide phenomena, can cause enormous drawbacks involving human-related activities, causing damage either to the infrastructure like buildings, road networks, and railways or even causing loss of human life. The continuous expansion of the built environment on an otherwise natural mountainous terrain makes the risk assessment of rockfalls compulsory. However, the unpredictability

of the phenomenon, the complexity of the triggering mechanisms, and the multifactorial reasons affecting rockfall paths make rockfall analysis challenging [2]. The study of rockfall risk needs integrated data collection and interdisciplinary techniques for sufficient analysis and interpretation [3–6].

Over the last few years, extensive studies have been accomplished on rockfall susceptibility assessment using several techniques. Since the 1980s, with the increasing popularity of GIS software and hardware, landslide susceptibility mapping has been developing [7–9]. Researchers throughout the globe have been experimenting by utilizing multicriteria methodologies within spatial environments to locate areas with potential slope instability and produce susceptibility maps [10–13]. Nowadays, different qualitative and quantitative methods, whether using heuristic hazard assessment techniques [14] or statistical and deterministic approaches [15–17], can be distinguished [18]. In addition, the high-resolution data derived from remote sensing techniques involving several types of satellite imagery have become necessary tools for applying those mentioned above [19–22].

In the case of Kalymnos Island and taking into consideration the large dispersion of the climbing sites, which cover relatively small areas, the demand to focus on very localized disastrous phenomena has led to the constantly increasing need for very-high-resolution topography data. Consequently, the generation of ultra-high-density point clouds, which include the elevation information followed by the earth's surface color data that are, in turn, used to construct Digital Surface Models (DSMs) and Ortho-photo-mosaics, became more than necessary. We utilized close-range remote sensing data acquired from UAS and high-resolution satellite imagery, which have been widely used in hazard mapping and risk assessment concerning floods [23], forest fires [24], soil erosions [25,26], rockfalls [27,28], etc. Most frequently, they are involved in several stages of data processing, especially when mapping steep-slope landscapes, which contain geological structures commonly exposed to natural geomorphic mechanisms such as erosional processes and, by extension, to landslides and rockfalls, posing safety hazards to people and infrastructure [29]. Considering the challenging, inaccessible terrain of Kalymnos and the need for dense field measurements to achieve reliable statistical analysis, traditional surveying methods with a standard geological compass are difficult to apply, underscoring the importance of close-range remote sensing techniques [30–33].

The contemporary analysis of rockfalls requires primarily the use of DSMs and Ortho-mosaics, which can be provided from long-range or /and close-range remote sensing data processing. The most applicable method for rockfall monitoring, quantitative analysis, and risk management is the employment of Light Detection and Ranging (LiDAR) datasets, either airborne [34] or terrestrial [35], or both after merging point-cloud datasets generated from different sources [36–39]. A more low-cost technique that is adaptable to harsh conditions is the Structure-from-Motion (SfM) approach, applied to acquired data with the use of Unmanned Aerial Systems (UASs), which along with Multi-View-Stereo (MVS) algorithms, enable automatic reconstruction of surface models in three dimensions [40].

In this work, we describe the study of the rockfall risk in Kalymnos Island (Figure 1), with different techniques. The primary goal was to limit the areas requiring detailed integrated simulations, which was achieved by producing a vulnerability map for the entire island that highlighted the highest-risk zones. We merged the resulting outcomes from (i) classical geological field mapping, (ii) the interpretation of high-resolution satellite data (WorldView-3 satellite images) for locating the spatial distribution of boulders but also for tracing the contemporary land cover, (iii) the integration of geoinformation data through an analytical hierarchy processing (several layers of induced spatial information have been constructed and correlated with each other within a GIS platform), (iv) close-range remote sensing campaigns with Unmanned Aerial Systems (the construction of more than a dozen of 3D models at the highest risk areas), and (v) an integrated simulation of rockfall events (sophisticated parametrization of software providing the analysis of different scenarios producing rock dispatches).

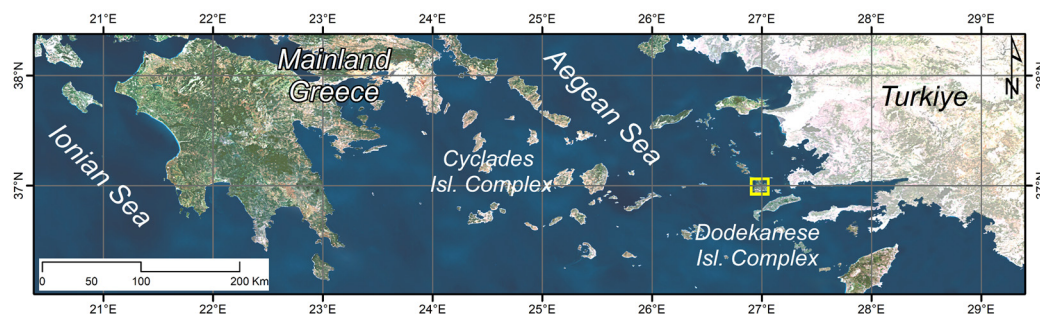


Figure 1. Index map of Kalymnos Island location (yellow rectangle) within the Aegean Sea.

2. Materials and Methods

The suggested workflow begins with the collection of spatial data that are related to rockfall phenomena [41], which are very frequent due to earthquakes that happen very often in this very active region of the Aegean [42], but also due to severe weather events that have been observed in the Eastern Mediterranean Sea [43,44]. This section includes a description of the collected and used data and the background theory of the methods used for rockfall susceptibility modeling. Utilizing these, data including the landslide susceptibility map and landslide conditioning factors were prepared and processed to generate new datasets for constructing and validating the models. The validation of the multidisciplinary study, in conjunction with a back-analysis approach applied to specific rockfall cases (for which there is no historical information for the time and the applicable circumstances), provided the opportunity to draw valuable conclusions regarding the vulnerability of rockfalls around the island of Kalymnos, especially at sports rock-climbing sites.

2.1. High-Resolution Satellite Image Interpretation

We used recently acquired (4 March 2021) commercial natural color WorldView-3 imagery (WV-3), which was downloaded through the MAXAR platform in the frame of the “SecureWatch” service, access to which was kindly provided to authors. A 3-band true-color, orthorectified, pansharpened image at pixel size dimensions of 0.3 m and downsampled at the 8-bit radiometric resolution, covering most of the onshore part of the island, was used as a base map for the detection of rock falls as well as the digitization of roads and buildings around the island.

The ortho-rectified WV-3 image was imported into a GIS environment, and a geo-database was created containing three different layers for roads (polyline features), buildings (polygon features), and boulders (point features). The latter was designed in a way to receive entries of point features, related to the fallen rock locations (Figure 2). The exact locations of boulders that had rolled downhill from the steep slopes around the island with minimum dimensions of 3 m were recorded, along with a series of spatial characteristics that enriched the geo-database concerning these point features (e.g., lithology, slope, distance from infrastructure, etc.).

During the data entry of boulder location points, the map viewing scale was held unchanged at 1:2000 and the cursor was set with a circle with a 3 m diameter. The latter allowed us to estimate the dimensions of each boulder and digitize only those that exceed 3 m in diameter. More than 7500 entries were input in the geo-database corresponding to fallen boulders, which had been dispatched from the basement and scattered around the island. It is more than evident that there are areas with a higher concentration of rockfalls, even though there are large boulders almost all over the island.

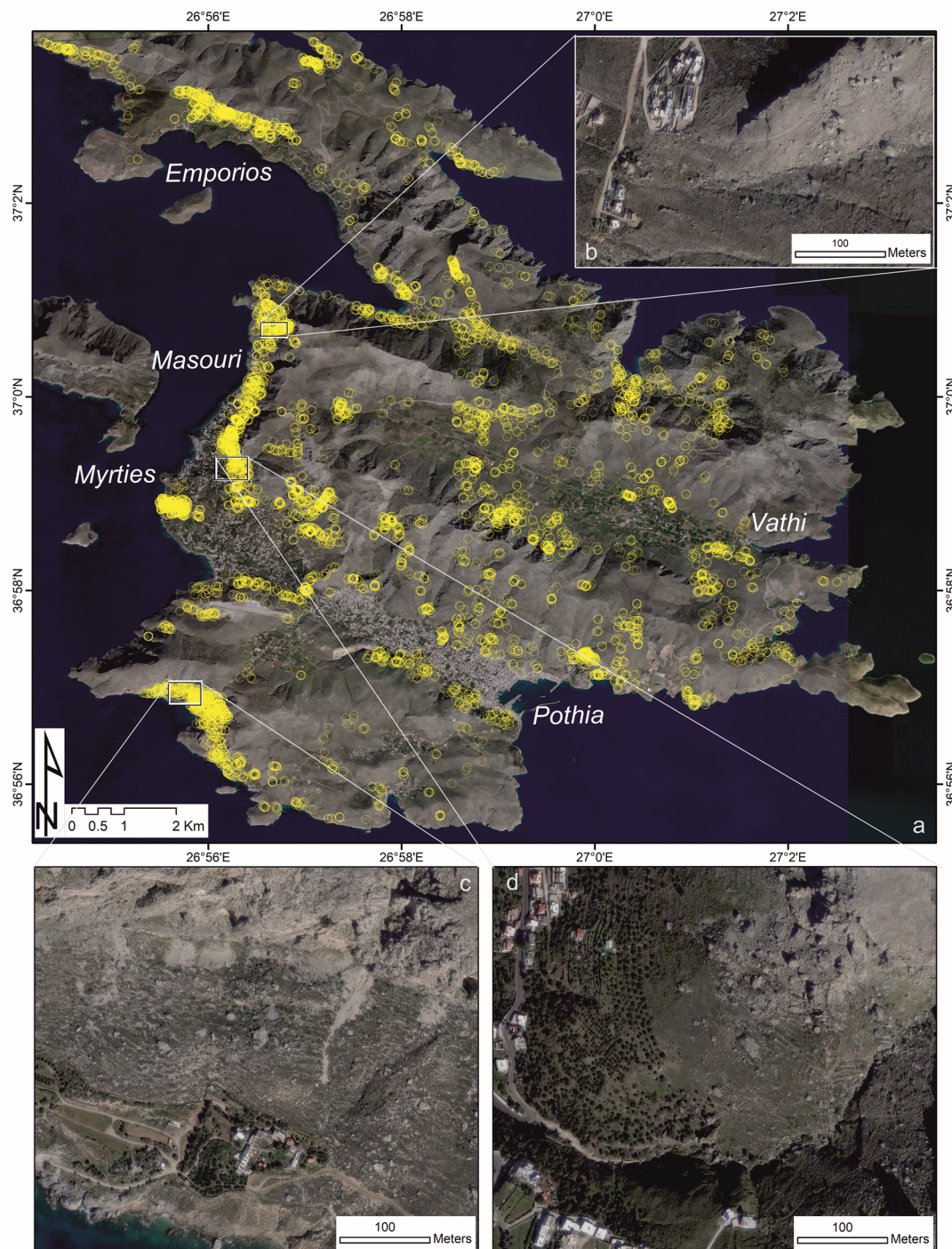


Figure 2. WorldView-3 imagery was used as a base map for locating boulders that were dispatched from the rock basement (a). More than 7500 boulders (yellow circles) were added to a geo-database during the interpretation stage. Three areas are presented magnified as example insets, in which 145 (b), 202 (c), and 151 (d) boulders larger than 3×3 m have been identified.

2.2. High-Resolution Topography

Since local topography is a crucial factor for initiating and generating a rockfall path, the need for an accurate and high-resolution Digital Terrain Model (DTM) is obvious. Therefore, a 2 m resolution DTM of the area was used, acquired from the Hellenic Cadastral, which is a national agency that provides the geodetic and cartographic coverage of Greece. Further processing of the DTM led to the generation of other layers of geoinformation,

such as the slope, which was also utilized for the estimation of the rockfall susceptibility of Kalymnos (Figure 3).

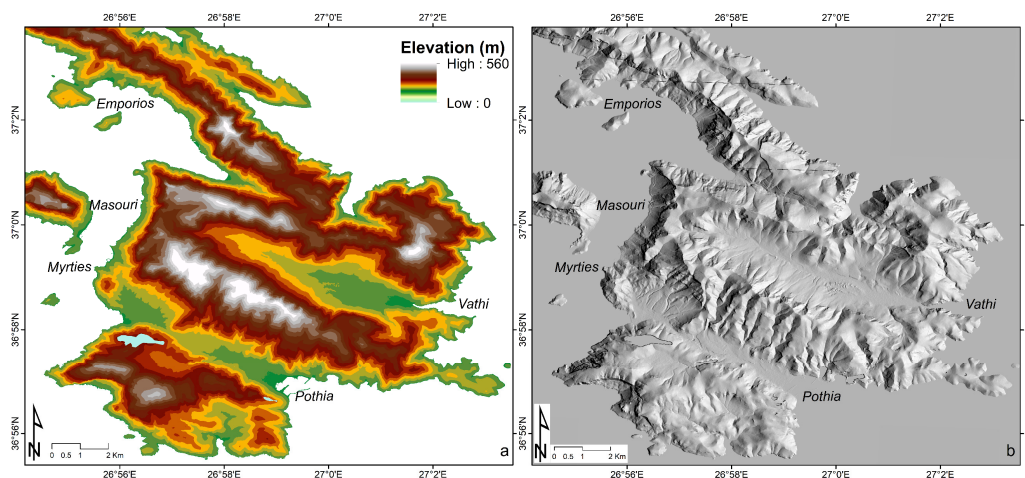


Figure 3. The high-resolution (2 m) DTM was processed (a) and a hillshade (b) was created, providing detailed information for the morphology of the island.

2.3. Geological Mapping and Field Observations

Kalymnos Island belongs to the Dodecanese Island complex, which is located on the SE Aegean Sea (Greece). Extended outcrops of carbonate rock units form vertical slopes, which are ideal for climbing and this is the main reason it is considered one of the most famous rock-climbing terrains in the world.

According to the geomorphological aspect, Kalymnos consists of several elongated higher relief units intercalated with lower elevation belts, arranged in an NNW–SSE orientation (Figure 3). The central range is the highest and is flanked by valleys to the north and south, while the northernmost range extends as a long peninsula projecting northwestward, with steep slopes along its entire length [45]. The quite deep ravines and rugged peaks yield significant tectonic activity across the whole onshore landscape of the island. The impressive relief hides an extensive karstic network, with several cavities and surface karst indicators at the carbonate rocks. Many caves have been explored, and despite their volume, the speleotheme decorations are impressive. Overall, it is characterized as an important geoh heritage site, with increased geodiversity.

From a geotectonic point of view, the Kalymnos rocks are part of the internal Hellenides [46,47]. After extensive fieldwork, an updated geological map was created (Figure 4), in which three geotectonic units were distinguished. The lowermost unit of the island is the Kefala Unit, which comprises a late-Paleozoic–Triassic low-grade carbonate sequence overlain unconformably by a Triassic flyschoid formation consisting of quartzites, radiolarites, reddish slates, conglomerates with blocks of fossiliferous marbles (Figure 5c), and gabbroic rocks [48]. Kefala Unit is overthrust by the high-grade metamorphic rocks of the Marina Basement Unit, which includes amphibolites, orthogneisses, and quartzites. The uppermost unit of the island is the Marina Cover Unit, a non-metamorphosed sequence of Mesozoic carbonates consisting of late-Triassic–mid-Jurassic shallow water dolomite and limestone, followed by late-Jurassic–early-Cretaceous cherty limestones (Figure 5a), overlain unconformably by late-Cretaceous limestones [49]. The two underlying units are juxtaposed against the Marina Cover Unit with a low-angle normal fault with top-to-SE shear sense (Figure 5d). Along the contact of the dolomite with the overlying limestone, an extended network of (sub-)vertical cliffs is developed, accompanied by intense rockfall phenomena due to differential weathering of these two carbonate lithologies (Figure 5b).

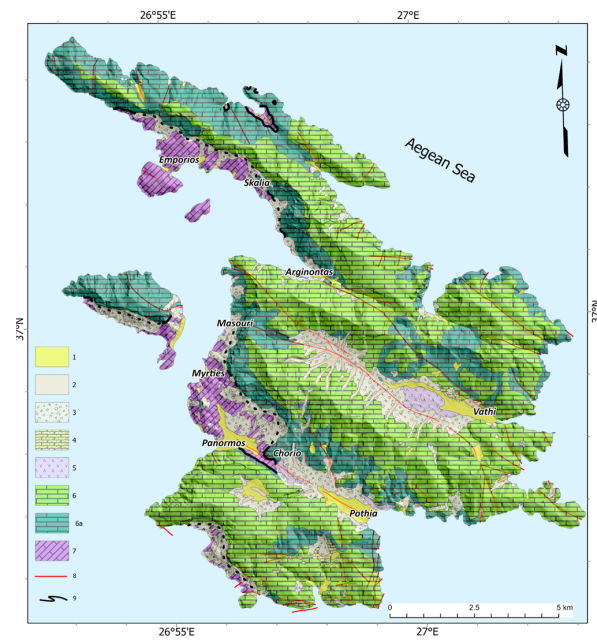


Figure 4. Simplified geological map of Kalymnos Island (modified from [48,50]). Post-Alpine sediments: alluvial deposits (1), recent debris (2), scree, rockfalls, and boulders (3), Neogene marine conglomerates and sandstone beds (4), quaternary volcano-sedimentary tuffs (5). Alpine basement: late-Triassic dolomites (6a) and late-Triassic–Cretaceous limestones (6) of Marina Cover Unit, Undifferentiated Marina Basement and Kefala Units (7). Fault (8). Detachment (9).



Figure 5. The most significant lithologies contributing to the steep geomorphology and hosting the climbing routes. (a) Upper stratigraphic section of the Marina cover Unit. Late-Jurassic–early-Cretaceous dark cherty limestone overlain unconformably by white to light grey massive late-Cretaceous limestone. (b) View of the climbing routes at the northern side of Arginonta Bay and the lower stratigraphic section of the Marina cover Unit. The smooth topography of the underlying dolomite (Dol) makes a stark contrast with the subvertical cliffs of the late Triassic limestone (Cal). (c) Late Permian fossils of *Fusulinidae* sp. (black arrow) in the white Permian marble of Kefala Unit. (d) View of the Detachment surface at northwest Kalymnos (red dashed line). The foliated cataclasite marks the south-dipping low-angle normal fault at the base of the Marina Cover Triassic limestone. (e) Garnet-mica schist of the Marina Basement Unit (black arrows pointing to garnet grains—Grt).

2.4. Land Cover and Use

The rationale behind incorporating land cover and use in rockfall vulnerability risk assessment models is that researchers often care about the safety of human presence and infrastructure, not nature itself [9]. Regarding land use, we require up-to-date information about the current state of the land surface. This is often achieved through visual interpretation of recent aerial photographs or, depending on the interpretation scale, through automatic or semi-automatic processing of satellite imagery [51,52].

We used a sub-dataset for the island of Kalymnos, named “CLC+ Backbone Raster Product”, which was created by the Copernicus program (Corine 2020) and modified after a minor update with image interpretation of the WV-3 image (see Section 2.1). It is a polygon vector dataset primarily based on the supervised classification of Sentinel-2 L2A satellite images acquired between July 2017 and June 2019. A series of land cover classes were identified, including several types of cultivated areas, sparse or no vegetation territories, and various types of manmade infrastructure (Figure 6).

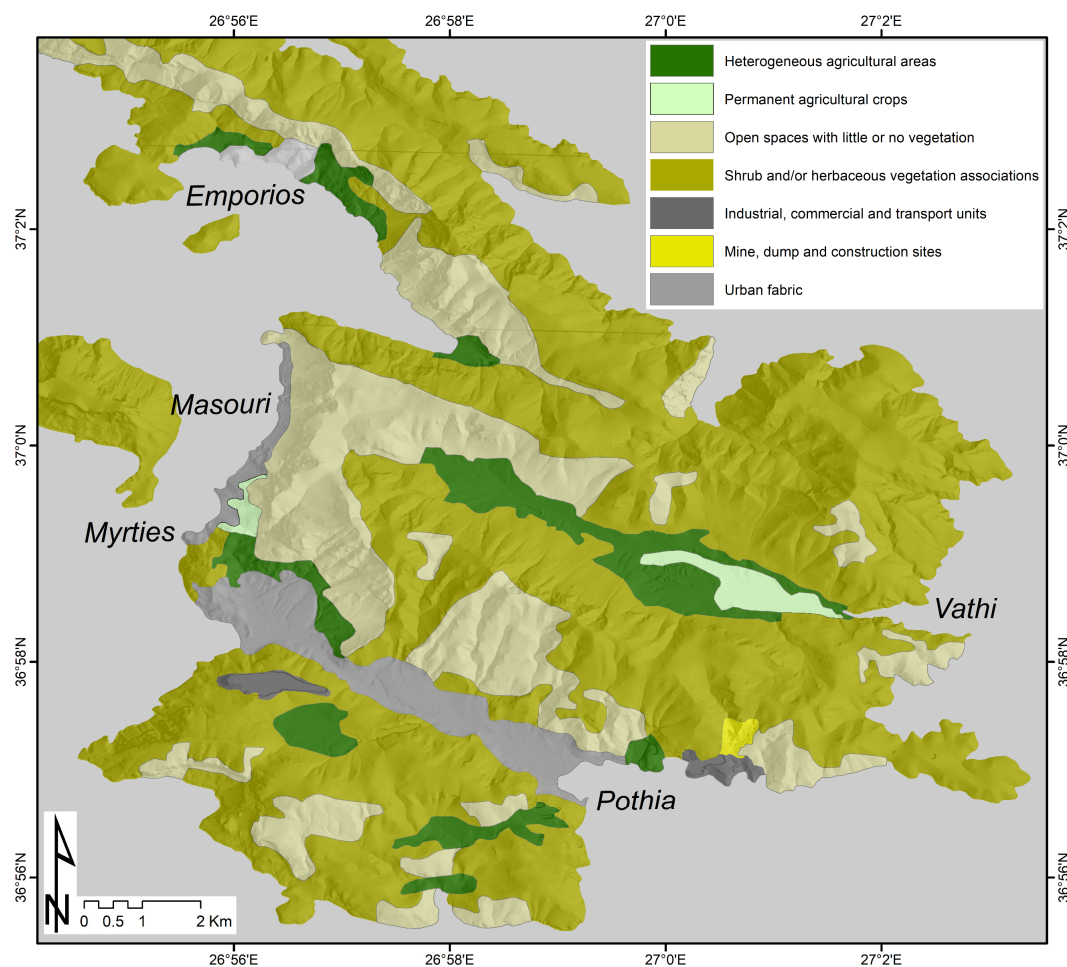


Figure 6. Land cover map modified from Corine 2020 dataset.

2.5. Sport Rock Climbing Sites

During the last two decades, Kalymnos has become a worldwide famous destination for sport rock climbing. More than 4000 routes have been marked on the almost vertical limestone cliffs, at about 150 sites (crags) spread around the island. Even though the locations of those sites cannot be part of the spatial processing, regarding the rockfall vulnerability risk assessment, it is a valuable information layer that should be seriously considered during the safety measures design if they are located in high-risk areas. The latter becomes higher due to the frequent presence of climbers.

3. Results

The workflow consists of several phases including data collection, processing, and further interpretation and analysis of a series of datasets leading to the proposal of safety measures, especially in high-priority areas (Figure 7).

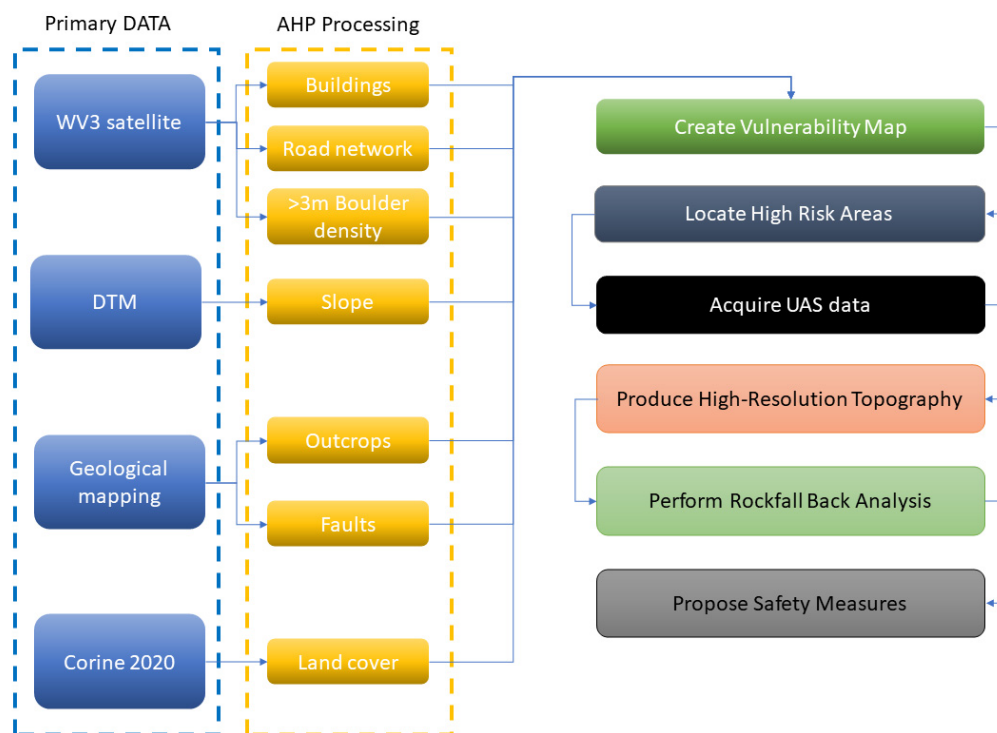


Figure 7. Flowchart describing the use of collected data within the proposed methodology.

3.1. GIS Layers Classification

Since the seven most critical layers have been collected, rasterized, and co-registered, the next step is to create classes of significance regarding the rockfall vulnerability risk and include this information in the database of each entity of the layers. A classification into five distinct classes was followed based on how each feature contributes to the rockfall risk. Each class is assigned a score from 1 to 5, corresponding to the characterization from “Very Low” to “Very High”, respectively.

Distance to build environment: Human infrastructure (buildings, hotel establishments, and water reservoirs) and, by extension, human lives, are considered one of the main factors for evaluating the rockfall vulnerability risk. This information is considered up to date as it was derived from the recently acquired WV3 imagery. The critical distance from the buildings was set at 100 m, and a dissolved buffer zone was created around the initial polygons, producing new ones. The areas within the new polygons were classified as “Very high” risk, whilst the areas outside them were classified as “Very low” (Figure 8a).

Distance to road network: Regarding road networks, human activities related to them, e.g., road constructions, extensive excavations, and deforestation, can cause significant rockfall phenomena [53]. Additionally, the risk near the main roads has increased dramatically. A distance map for the digitized road polylines was generated using the Euclidean distance method from the road network, dividing it into areas within and outside a dissolved buffer zone of 100 m on each side of the central line. By following the previously mentioned method of classification, the areas inside the new polygons were classified as “Very high” risk, whilst the areas outside them were classified as “Very low” (Figure 8b).

Boulder density: The boulder locations reveal the areas of high rockfall potential and the result of the topography dynamics. Therefore, a new layer was produced based on the point features that have been digitized all around the island, taking into consideration the

frequency of the rockfalls and representing the density. Simultaneously, the fields of the database were filled with more necessary information (distance from infrastructure, slope at the location, lithology, etc.), received by using other GIS layers that have been described in previous sections. The geospatial algorithms used to calculate the boulder density led to the generation of a classified raster layer. The latter has five distinct classes introducing “Very low” to “Very high” risk, depending on the number of points found in a radius of 100 m, as this was the pixel size of the layer (Figure 8c).

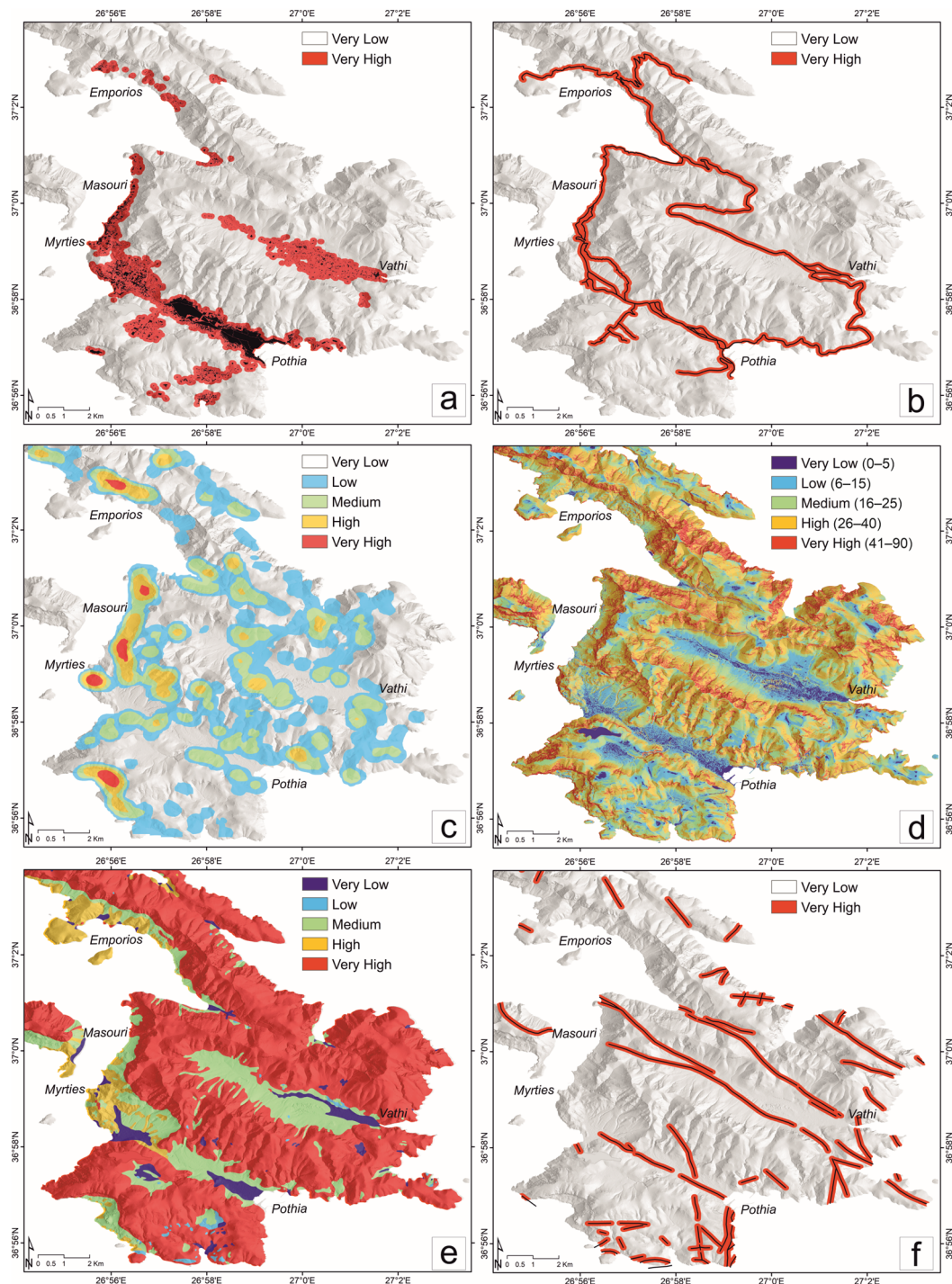


Figure 8. The classification of the main layers regarding their potential to contribute to rockfall risk. (a) Human infrastructure, (b) main road network, (c) boulder density, (d) slope angle, (e) lithology, and (f) fault proximity.

Slope: Topography is considered one of the critical factors that affect landslides and rockfalls [54] as it controls the shear forces acting on the relief. Gentle (low gradient) slopes are expected to decrease the risk of rockfalls to zero, whilst steep (high gradient) slopes are expected to increase the risk of rockfalls to high. Kalymnos is an area of high steepness where the slope can reach almost 90 degrees. The slope angle was modeled using a grid-based DEM and was classified into five classes related to risk; (a) very gentle slopes of 0–5° as “Very low”, (b) gentle slopes of 6–15° as “Low”, (c) moderate steep slopes of 16–25° as “Medium”, (d) steep slopes of 26–40° as “High”, and (e) very steep slopes of 41–90° as “Very high” (Figure 8d).

Rock type: Lithology is one of the most influential and critical controlling factors of rockfalls since it leads to differences in the stability and resistance of rocks and displays different susceptibility rates [55]. The lithology layer was classified into five distinct classes of “Very low” to “Very high” risk, depending on the type of rocks and the potential of each type to be involved in a rockfall by dispatching large particles of the undisturbed beds. Therefore, in terms of rockfall vulnerability risk, the alluvial deposits were classified as “Very low”, the Neogene beds were classified as “Low”, the recent debris, scree, and tuffs were classified as “Medium”, the metamorphic carbonates and schists were classified as “High”, and the non-metamorphic carbonate rocks were classified as “Very high” risk (Figure 8e).

Proximity to faults: The development of cracks and shear fractures along the fault zones has a serious role in the stability of rocks [56]. Rock mass movements commonly occur in fault zones and the possibility of rockfall events increases. The fault layer was derived by digitizing polylines on published geological maps [50] and updating them during fieldwork. A distance map for the digitized fault polylines was generated using the Euclidean distance method from the fault trace, dividing it into areas within and outside a dissolved buffer zone of 100 m at each side of the central line. By following the previously mentioned method of classification, the areas inside the new polygons were classified as “Very high” risk, whilst the areas outside them were classified as “Very low” (Figure 8f).

Land Cover: The type of land use indirectly affects slope stability and is a potential driver of rockfalls. Vegetated regions enhance slope stability through their effect on the soil’s hydrological and mechanical attributes [57]. The land use/cover polygon data were classified into five classes based on their properties and how they could be affected by rockfalls. Therefore, regarding rockfall vulnerability risk, the effect on manmade infrastructure (industrial, commercial, and transport units; urban fabric; mine, dump, and construction sites) is characterized as “Very high”, whilst cultivated areas (heterogeneous agricultural areas; permanent crops) were classified as “High”, shrub and/or herbaceous vegetation associations areas were classified as “Medium”, and open spaces with little or no vegetation was classified as “Very low”.

3.2. Analytical Hierarchy Process (AHP)

The next step of processing involves the transformation of the spatial data into raster layers, which in turn are used within an Analytical Hierarchy Process. This is a decision-making process based on the prioritization of several criteria [58]. The first stage in establishing priorities is to conduct pairwise comparisons between layers at the same hierarchical level. These comparisons are carried out through logical and empirical evaluations by the operator, establishing concrete comparative judgments. The next step involves systematically constructing hierarchies and establishing priorities by ensuring logical coherence in terms of effectively organizing and evaluating spatial relationships. Through this AHP, the relationship between the given criteria is structured hierarchically in a comparison matrix, aiming to subjectively score the importance of each one by calculating factors (we used an online environment [59]). Numerical values are assigned to fill the pairwise comparison matrix, representing the relative importance of one piece of spatial geoinformation compared to another with respect to a specific property (Table 1).

Table 1. Matrix of the resulting weights based on pairwise comparisons between the selected geospatial layers (Principal eigenvalue = 7.730). The bottom line shows the weighted influence of each raster layer for the calculated risk value.

	Slope	Roads	Faults	Geology	Landcover	Buildings	Boulders
Slope	1.00	5.00	7.00	4.00	7.00	3.00	0.14
Roads	0.20	1.00	3.00	0.50	3.00	1.00	0.14
Faults	0.14	0.33	1.00	0.20	0.50	0.25	0.14
Geology	0.25	2.00	5.00	1.00	4.00	1.00	0.14
Landcover	0.14	0.33	2.00	0.25	1.00	1.00	0.14
Buildings	0.33	1.00	4.00	1.00	1.00	1.00	0.14
Boulders	7.00	7.00	7.00	7.00	7.00	7.00	1.00
Weighted factors	0.21	0.06	0.03	0.09	0.04	0.07	0.51

In the final step, a GIS raster calculator engine is used, in which the “Vulnerability” of each pixel is calculated. With this tool, GIS users can utilize raster layers as variables to create mathematical expressions, which can incorporate mathematical operators. The result is computed as a mathematical function summing the input image pixel values (1 to 5) for each one of the seven raster layers, multiplied by the AHP weighted factors, respectively.

Therefore, a vulnerability map is generated (Figure 9), which in turn should be validated either remotely, by using the VHR satellite images, or by fieldwork where necessary. Both validation methods show a high relation between high-risk areas and rockfall occurrence (Figure 10). Field campaigns including Unmanned Aerial System flights and image data acquisition were scheduled in these areas to produce detailed topography. The latter was used in the next step of the methodology to perform back analyses at specific boulders, and after rolling back their trace, the dispatching points were revealed. This led to the suggestion of measures that increase the sense of safety for tourists and the local community, always taking into consideration sport climbing sites that have been a popular attraction on the island for the last 25 years or so.

Table 2. Information and specifications of each of the 12 flights that were carried out during the image acquisition.

Code	Number of Images	Flying Altitude (m)	DSM Resolution (cm)	Ortho-Image Resolution (cm)	XY Error (cm)	Z Error (cm)
A10	269	77	3.8	1.9	1.86	2.29
B10	322	114	5.6	2.8	1.98	1.04
E10	246	122	7.7	3.8	2.45	5.38
M10	639	138	6.8	3.4	1.95	2.73
M20	314	207	9.9	5.0	1.71	1.49
M30	515	211	10.2	5.1	2.39	2.49
M40	377	104	5.3	2.7	1.95	1.49
P10	225	130	6.4	3.2	2.28	2.75
P20	254	87	4.4	2.2	1.83	1.69
P30	527	117	5.7	2.9	1.49	1.55
P40	555	143	6.7	3.4	1.59	2.63
P50	485	96	4.8	2.4	2.09	1.84

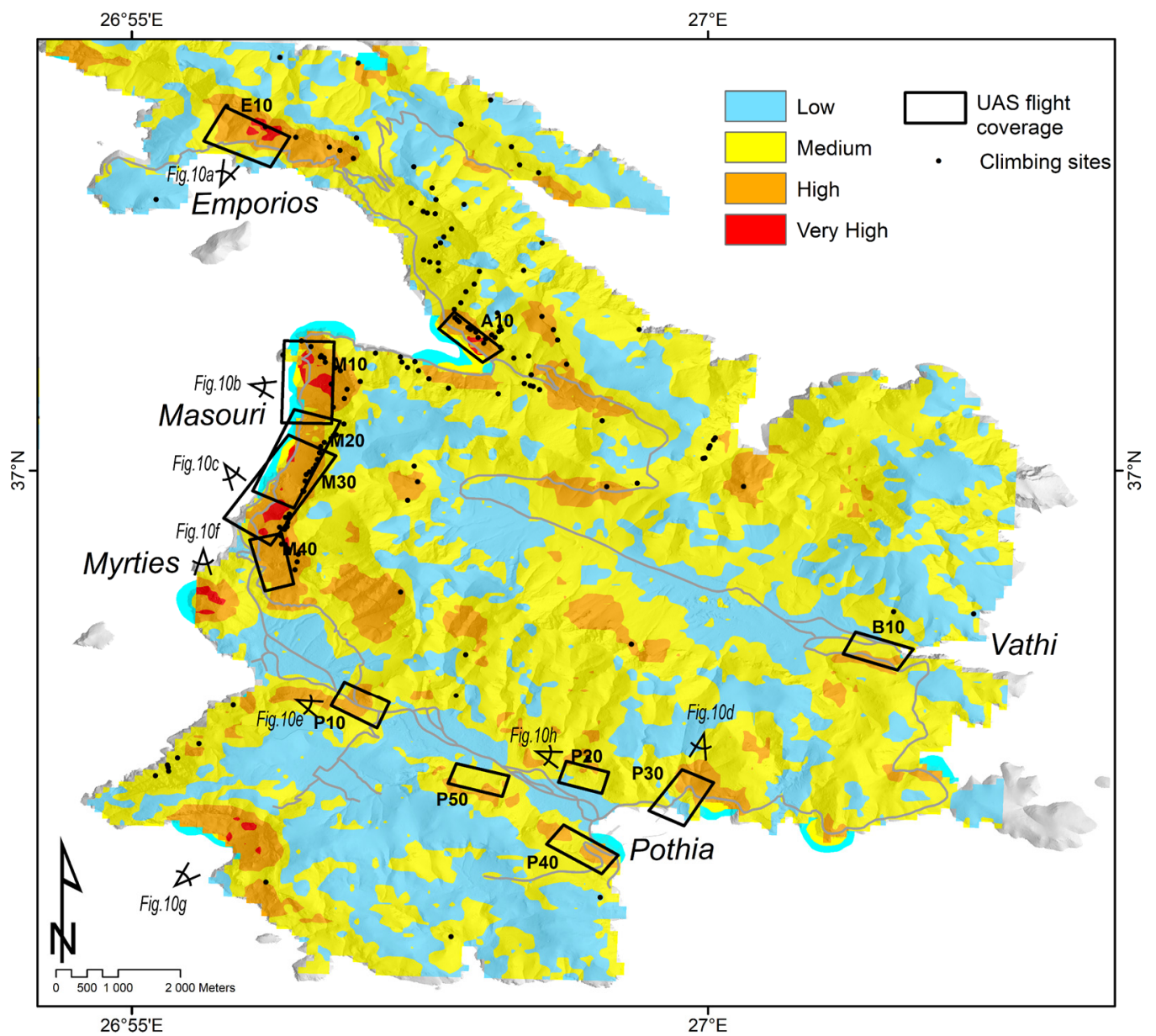


Figure 9. Vulnerability map for the island of Kalymnos regarding the rockfall risk. Red and orange colors define the “Very High” and “High” risk areas. The field validation showed an impressive relationship with reality. Note the photograph locations and angles of Figure 10. The black rectangles show the coverage of a detailed study with close-range remote sensing using UAS (see Table 2), whilst black dots represent the sport climbing sites.

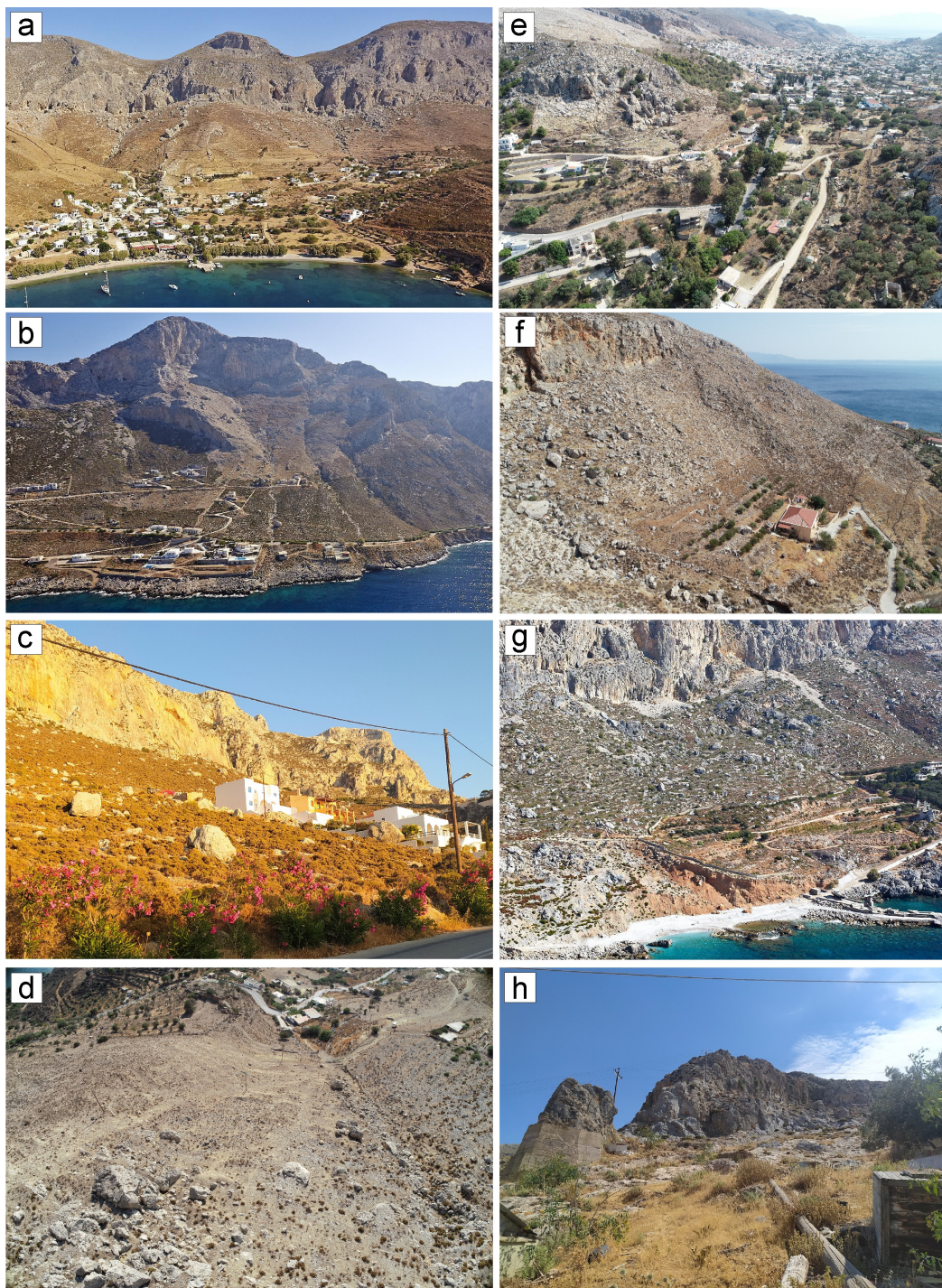


Figure 10. Aspects of the most characteristic “Very High” rockfall risk areas as they have been spatially calculated through vulnerability map generation (see Figure 9 for locations). (a) Subvertical cliff and large boulders uphill from the residences. (b) Large boulders are hanging over residences, with some already situated among them. (c) Closer look of numerous large boulders among residences. (d) A top-down view from the cliff reveals fallen boulders scattered down the slope, some tumbling toward the residences below, appearing dangerously close to impact. (e) View of the limestone bedrock collapse showing freshly fallen boulders breaking away from the cliff face. (f) Loose boulders slide down near residence. (g) Fallen boulders uphill the Holy Trinity monastery (south Kalymnos). (h) Steep cliff and poor measures right next to the edge of the town.

3.3. Close-Range Remote Sensing Using UAS

Taking into consideration the most vulnerable areas that were indicated by the constructed vulnerability map along with the validation results, a close-range remote sensing campaign was conducted with a rotor-wing UAS (DJI Phantom 4 Real-Time Kinematic) (DJI, Shenzhen, China) equipped with a stabilized, built-in 20Megapixel camera (of 8.8 mm focal length) bundled on a two-axis gimbal. This unmanned platform was chosen due to its relatively reasonable cost and easy on-site operation in combination with the equipped miniaturized Geodetic Navigation Satellite System (GNSS) antenna, which provides sufficient precision, particularly for the horizontal positioning required to facilitate the proper alignment of the images captured during the survey [60]. Although ground control points (GCPs) are a vital tool for ensuring geolocation accuracy, in this case study, in which the morphology of the high-risk areas consists of very steep slopes with limited accessibility, the use of the RTK antenna with which the drone is equipped was considered to be efficient enough for highly accurate results. Nevertheless, we used the GNSS receiver in the Network Real-Time Kinematic (NRTK) mode connected to the SmartNET provider accuracy service [61] to obtain subjective geolocation, which is also necessary for comparing independent surveys.

The UAS flight survey was designed to cover 12 areas around Kalymnos for a total of 5.71 km², where—based on the process of the geospatial data—the largest rockfall risk was calculated. Two survey-planning methods were applied to these areas depending on the morphology and slope of the relief. The first planning method was designed with multi-oriented 3D photogrammetry (Figure 11a) in which a flight path is followed with the camera pointing in the nadiral direction, followed by four flight paths with images captured at different camera angles (oblique) for a total of five segments. It was applied to relatively small areas with visibility from different azimuth directions (e.g., small hills) but also where a higher spatial resolution was necessary. The second planning method was designed with double-grid flightpaths, normal to each other, and the images were also captured at oblique camera angles (~60°), depending on the morphological slopes of the target area (Figure 11b). This method provides high-resolution data in 3D as well and is indicative for larger areas, especially when the roughness of the anaglyph is high.

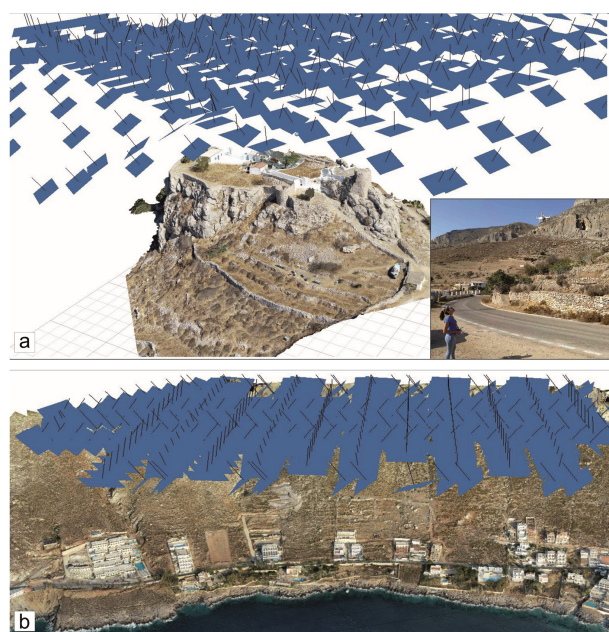


Figure 11. The areas of interest were captured using different methods, depending on the complications of the earth's surface. (a) Multi-oriented image data acquisition method, in which the area of interest needs to be captured from four directions. (b) Double-grid flightpath method, with images acquired from two oblique directions normal to each other.

During every single flight, a large number of images were acquired, which were processed within Agisoft Metashape v.2.0 photogrammetry software [62], to produce high-resolution DSMs and ortho-mosaics, based on dense point clouds consisting of tens of million points each (Table 2).

3.4. Integrated Simulations

Using the advanced software Rocfall2 [63], we conducted modeling and integrated simulations to confirm the density and distribution of previously recorded boulders from past rockfalls and estimate the trajectories of potential future events. Rocfall2 is sophisticated two-dimensional analysis software, designed to assess the risk of rockfalls in natural and artificial slopes to determine the required measures. The software creates numerous repeated simulations of rockfalls and calculates specific parameters such as the boulders' energy, speed, bounce height, and endpoint on slopes of a given geometry. These simulations are based on the geomaterial of the bouncing boulder (e.g., lithology), the friction angle, the roughness of the ground (roughness), and the angular velocity of falling boulders.

The rockfalls were simulated along several profiles (sections) in each one of the 12 high-risk areas (description in Table 2 and location in Figure 9). The very-high-resolution DSMs, which were generated using the SfM method (see Section 3.3), were employed to define the topographical geometry, a critical factor for accurately simulating each rockfall event. Estimating the boulder trajectory required the precise determination of several other factors, such as the point of detachment, the initial speed, and the geotechnical parameters along the trajectory. As the boulders meet the earth's surface, their kinetic energy (e.g., normal and tangential speed component) is reduced according to the applied rebound coefficients R_n (vertical) and R_t (tangential), which directly depend on the geomaterial. The design parameters are within the range suggested in the literature. The maximum mass of a detached boulder was equal to 70 tn, corresponding roughly to a boulder 27 m³ in volume (to be comparable with the dimensions of the boulders that comprise the geo-database described in Section 2.1). The estimated trajectories are considered realistic.

For each one of the 12 high-risk areas, we simulated several rockfalls along specific profiles (Figure 12) and estimated the distribution of endpoint locations. Within the software, we adjusted the parameters of the fallen particles to ensure they were immobilized at the locations identified through satellite image interpretation. Additionally, we calculated the total kinetic energy of boulders and the bounce height envelope of boulders along the profile. These results allowed us to propose specific measurements for the safety of climbers and infrastructure.

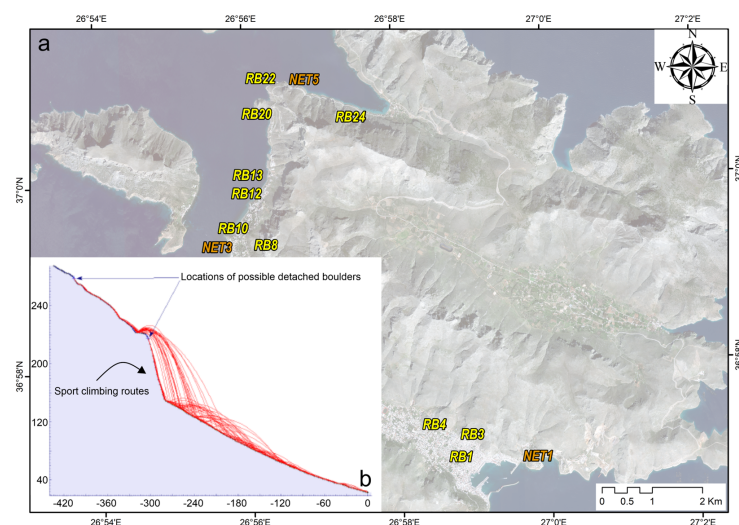


Figure 12. (a) Distribution of the proposed “first priority” safety measures. Barrier locations are yellow, while mesh nets are orange. (b) The inset shows an example of numerous rockfall simulations, which were performed at the climbing sites characterized as high-risk areas.

4. Discussion

Previous research on vulnerability risk assessment to rockfalls has primarily concentrated on detailed mapping of steep slopes to evaluate infrastructure vulnerability. In this study, however, the focus was shifted to assessing the risk at sport rock-climbing sites established around the island of Kalymnos, which present unusually high human concentrations nearly year-round.

By evaluating the extent of the climbing sites, their natural geomorphological features (such as steep slopes), and their geographic location regarding the geological outcrops, we can gain a deeper understanding of the risk for human loss due to rock failures, even though these sites have high potential as alternative tourist attractions. This assessment allows us to gauge human safety within the tourism industry on a larger scale, offering a scientific foundation for tourism planning and development.

The high-precision, real-scene 3D model of such steep landscapes described in this work not only fulfills research requirements in academic studies, tourism development, and spatial planning but also incorporates detailed geomorphological information, enabling more accurate replication of the real-world and consequently quantifying the rockfall risk accordingly. When integrated with virtual reality technology, these models can enhance interactivity and contribute to a safer environment, making it highly valuable for promoting sport-climbing tourism.

The application of the described methodology covering the entire onshore area of the island seems to delineate its most vulnerable parts to rockfalls, saving precious time for integrated simulations and designing safety measures. These can be applied to several locations on the island and are focused on preventing rockfalls from producing infrastructure damage. In general, conventional methods such as mesh and cable nets, as well as barriers, can prevent rocks from reaching manmade constructions (Figure 12). The latter would be established to keep the boulders from reaching the infrastructure in cases that the slopes—as a potential source of rockfalls—are being used as climbing sites, whilst nets would be installed at vulnerable slopes that are not used by climbers. Concerning the climbing sites that fall in the high-risk areas, it is recommended that they be systematically monitored and characterized with signs that inform the climbers of the dangerous rock failures that could cause further rockfalls.

Although the described workflow proves to be a very successful and prominent methodology, which is open for further discussion regarding improvements and modifications, there are some drawbacks. These mainly concern (i) the correctness of the initial data that are used within the AHP and (ii) the amount of time spent for accurate UAS data acquisition.

Although the described workflow is a highly successful and promising methodology that remains open to discussion for potential improvements and modifications, it has some drawbacks. These primarily involve (i) the questionable correctness of the initial data imported in the AHP (all kinds of mapping, boulder locations, etc.) and (ii) the considerable time required for precise UAS data acquisition. Additionally, challenges can arise in maintaining consistency across datasets, particularly when integrating data from multiple sources or repeated UAS flights over time. Variability in environmental conditions, sensor calibration, and operator expertise can all impact data quality, which, in turn, affects the reliability of the results derived from the integrated simulations. Furthermore, the high computational demands of processing large datasets can limit efficiency and may require significant amounts of time and resources.

5. Conclusions

As real-scene 3D technology advances, its applications expand across various fields, leading to an increasing demand for higher precision and quality in 3D models. In disciplines like geomorphology and geology, particularly in rockfall risk research, there is a pressing need to develop high-precision real-scene 3D models.

This paper integrates VHR satellite remote sensing and UAS remote sensing technologies, utilizing photogrammetry to develop a comprehensive method for constructing high-precision real-scene 3D models of steep slope landscapes and mapping the locations of boulders that have previously fallen from the almost vertical cliffs. The primary challenges in building these slope models are the complexity of the cliffs and the large size of the areas of interest. The paper proposes subdividing the entire region into smaller sections to overcome these challenges. This subdivision is achieved by applying Analytical Hierarchy Processing (AHP) to various factors within a GIS platform.

The successful implementation of this methodology offers valuable insights and technical guidance for future 3D modeling of other physical geographical landscapes. As technology continues to be refined and optimized, the field of close-range remote sensing holds significant potential for further development and research opportunities in rockfall risk assessment.

Author Contributions: Conceptualization, E.V. and E.L.; methodology, E.V., A.K., K.S., S.L. and J.L.; software, E.V., A.K., J.L. and E.K.; validation, E.V., A.K., J.L. and E.K.; formal analysis, A.K.; data curation, A.K.; writing—original draft preparation, E.V., A.K. and K.S.; writing—review and editing, E.V., A.K. and K.S.; visualization, E.V., A.K., J.L. and E.K.; supervision, E.V.; project administration, E.K.; funding acquisition, E.L. All authors have read and agreed to the published version of the manuscript.

Funding: This research received no external funding.

Data Availability Statement: The data presented in this study are available on request from the corresponding author. The data are not publicly available due to privacy.

Acknowledgments: The authors would like to express their sincere appreciation to four anonymous reviewers, whose comments contributed for the improvement of the initial manuscript.

Conflicts of Interest: The authors declare no conflicts of interest.

References

1. Spyrou, E.; Triantaphyllou, M.V.; Tsourou, T.; Vassilakis, E.; Asimakopoulos, C.; Konsolaki, A.; Markakis, D.; Marketou-Galari, D.; Skentos, A. Assessment of Geological Heritage Sites and Their Significance for Geotouristic Exploitation: The Case of Lefkas, Meganisi, Kefalonia and Ithaki Islands, Ionian Sea, Greece. *Geosciences* **2022**, *12*, 55. [\[CrossRef\]](#)
2. Saroglou, C.; Asteriou, P.; Zekkos, D.; Tsiambaos, G.; Clark, M.; Manousakis, J. UAV-based mapping, back analysis and trajectory modeling of a coseismic rockfall in Lefkada island, Greece. *Nat. Hazards Earth Syst. Sci.* **2018**, *18*, 321–333. [\[CrossRef\]](#)
3. Karantanellis, E.; Marinos, V.; Vassilakis, E. Object-based characterization of landslide phenomena using UAV photogrammetry. In Proceedings of the Regional Conference on Geomorphology (IAG), Athens, Greece, 19–21 September 2019.
4. Karantanellis, E.; Marinos, V.; Vassilakis, E.; Christaras, B. Object-Based Analysis Using Unmanned Aerial Vehicles (UAVs) for Site-Specific Landslide Assessment. *Remote Sens.* **2020**, *12*, 1711. [\[CrossRef\]](#)
5. Karantanellis, E.; Marinos, V.; Vassilakis, E.; Hölbling, D. Evaluation of Machine Learning Algorithms for Object-Based Mapping of Landslide Zones Using UAV Data. *Geosciences* **2021**, *11*, 305. [\[CrossRef\]](#)
6. Schilirò, L.; Robiati, C.; Smeraglia, L.; Vinci, F.; Iannace, A.; Parente, M.; Tavani, S. An integrated approach for the reconstruction of rockfall scenarios from UAV and satellite-based data in the Sorrento Peninsula (southern Italy). *Eng. Geol.* **2022**, *308*, 106795. [\[CrossRef\]](#)
7. Gupta, R.P.; Joshi, B.C. Landslide hazard zoning using the GIS approach—A case study from the Ramganga catchment, Himalayas. *Eng. Geol.* **1990**, *28*, 119–131. [\[CrossRef\]](#)
8. van Dijke, J.J.; van Westen, C.J. Rockfall hazard: A geomorphologic application of neighbourhood analysis with ILWIS. *ITC J.* **1990**, *1*, 40–44.
9. Carrara, A.; Cardinali, M.; Detti, R.; Guzzetti, F.; Pasqui, V.; Reichenbach, P. GIS techniques and statistical models in evaluating landslide hazard. *Earth Surf. Process. Landf.* **1991**, *16*, 427–445. [\[CrossRef\]](#)
10. Zhang, Y.; Yue, P.; Zhang, G.; Guan, T.; Lv, M.; Zhong, D. Augmented Reality Mapping of Rock Mass Discontinuities and Rockfall Susceptibility Based on Unmanned Aerial Vehicle Photogrammetry. *Remote Sens.* **2019**, *11*, 1311. [\[CrossRef\]](#)
11. Nicu, I.C. Application of analytic hierarchy process, frequency ratio, and statistical index to landslide susceptibility: An approach to endangered cultural heritage. *Environ. Earth Sci.* **2018**, *77*, 79. [\[CrossRef\]](#)
12. Tavoularis, N.; Papathanassiou, G.; Ganas, A.; Argyrakis, P. Development of the Landslide Susceptibility Map of Attica Region, Greece, Based on the Method of Rock Engineering System. *Land* **2021**, *10*, 148. [\[CrossRef\]](#)

13. Youssef, A.M.; Pradhan, B.; Dikshit, A.; Al-Katheri, M.M.; Matar, S.S.; Mahdi, A.M. Landslide susceptibility mapping using CNN-1D and 2D deep learning algorithms: Comparison of their performance at Asir Region, KSA. *Bull. Eng. Geol. Environ.* **2022**, *81*, 165. [[CrossRef](#)]
14. Barredo, J.; Benavides, A.; Hervás, J.; van Westen, C.J. Comparing heuristic landslide hazard assessment techniques using GIS in the Tirajana basin, Gran Canaria Island, Spain. *Int. J. Appl. Earth Obs. Geoinf.* **2000**, *2*, 9–23. [[CrossRef](#)]
15. Süzen, M.L.; Doyuran, V. A comparison of the GIS based landslide susceptibility assessment methods: Multivariate versus bivariate. *Environ. Geol.* **2004**, *45*, 665–679. [[CrossRef](#)]
16. Ayalew, L.; Yamagishi, H. The application of GIS-based logistic regression for landslide susceptibility mapping in the Kakuda-Yahiko Mountains, Central Japan. *Geomorphology* **2005**, *65*, 15–31. [[CrossRef](#)]
17. Nohani, E.; Moharrami, M.; Sharafi, S.; Khosravi, K.; Pradhan, B.; Pham, B.T.; Lee, S.M.; Melesse, A. Landslide Susceptibility Mapping Using Different GIS-Based Bivariate Models. *Water* **2019**, *11*, 1402. [[CrossRef](#)]
18. Wohlers, A.; Damm, B. Rockfall Vulnerability of a Rural Road Network—A Methodological Approach in the Harz Mountains, Germany. *Geosciences* **2022**, *12*, 170. [[CrossRef](#)]
19. Raucoules, D.; Fomelis, M.; Negulescu, C.; Michele, M.d.; Aunay, B.; Tomaro, F. Landslide Observation from ALOS-2/PALSAR-2 Data (Image Correlation Techniques and Sar Interferometry). Application to Salazie Circle Landslides (La Reunion Island). In Proceedings of the IGARSS 2018—2018 IEEE International Geoscience and Remote Sensing Symposium, Valencia, Spain, 22–27 July 2018; pp. 506–509.
20. Fomelis, M.; Raucoules, D.; Colas, B.; Michele, M.d. On the Effect of Interferometric Pairs Selection for Measuring Fast Moving Landslides. In Proceedings of the IGARSS 2019—2019 IEEE International Geoscience and Remote Sensing Symposium, Yokohama, Japan, 28 July–2 August 2019; pp. 9614–9617.
21. Xie, M.; Zhao, W.; Ju, N.; He, C.; Huang, H.; Cui, Q. Landslide evolution assessment based on InSAR and real-time monitoring of a large reactivated landslide, Wenchuan, China. *Eng. Geol.* **2020**, *277*, 105781. [[CrossRef](#)]
22. Vassilakis, E.; Fomelis, M.; Erkeki, A.; Kotsi, E.; Lekkas, E. Post-event surface deformation of Amyntaio slide (Greece) by complementary analysis of Remotely Piloted Airborne System imagery and SAR interferometry. *Appl. Geomat.* **2021**, *13*, 65–75. [[CrossRef](#)]
23. Skakun, S.; Kussul, N.; Shelestov, A.; Kussul, O. Flood Hazard and Flood Risk Assessment Using a Time Series of Satellite Images: A Case Study in Namibia. *Risk Anal.* **2014**, *34*, 1521–1537. [[CrossRef](#)]
24. Dong, X.; Li-min, D.; Guo-fan, S.; Lei, T.; Hui, W. Forest fire risk zone mapping from satellite images and GIS for Baihe Forestry Bureau, Jilin, China. *J. For. Res.* **2005**, *16*, 169–174. [[CrossRef](#)]
25. Vrieling, A.; de Jong, S.M.; Sterk, G.; Rodrigues, S.C. Timing of erosion and satellite data: A multi-resolution approach to soil erosion risk mapping. *Int. J. Appl. Earth Obs. Geoinf.* **2008**, *10*, 267–281. [[CrossRef](#)]
26. Drzewiecki, W.; Weżyk, P.; Pierzchalski, M.; Szafrńska, B. Quantitative and Qualitative Assessment of Soil Erosion Risk in Małopolska (Poland), Supported by an Object-Based Analysis of High-Resolution Satellite Images. *Pure Appl. Geophys.* **2014**, *171*, 867–895. [[CrossRef](#)]
27. Lan, H.; Martin, C.D.; Zhou, C.; Lim, C.H. Rockfall hazard analysis using LiDAR and spatial modeling. *Geomorphology* **2010**, *118*, 213–223. [[CrossRef](#)]
28. Karantanellis, E.; Marinos, V.; Vassilakis, E. 3D hazard analysis and object-based characterization of landslide motion mechanism using UAV imagery. *Int. Arch. Photogramm. Remote Sens. Spat. Inf. Sci.* **2019**, *XLII-2/W13*, 425–430. [[CrossRef](#)]
29. Nesbit, P.R.; Hubbard, S.M.; Hugenholtz, C.H. Direct Georeferencing UAV-SfM in High-Relief Topography: Accuracy Assessment and Alternative Ground Control Strategies along Steep Inaccessible Rock Slopes. *Remote Sens.* **2022**, *14*, 490. [[CrossRef](#)]
30. Migliazza, M.; Carriero, M.T.; Lingua, A.; Pontoglio, E.; Scavia, C. Rock Mass Characterization by UAV and Close-Range Photogrammetry: A Multiscale Approach Applied along the Vallone dell’Elva Road (Italy). *Geosciences* **2021**, *11*, 436. [[CrossRef](#)]
31. Zhang, J.-y.; Li, H.-b.; Yang, X.-g.; Jiang, N.; Zhou, J.-w. Quantitative assessment of rockfall hazard in post-landslide high rock slope through terrestrial laser scanning. *Bull. Eng. Geol. Environ.* **2021**, *80*, 7315–7331. [[CrossRef](#)]
32. Mazzanti, P.; Caporossi, P.; Brunetti, A.; Mohammadi, F.I.; Bozzano, F. Short-term geomorphological evolution of the Poggio Baldi landslide upper scarp via 3D change detection. *Landslides* **2021**, *18*, 2367–2381. [[CrossRef](#)]
33. Konstantinidis, I.; Marinos, V.; Papathanassiou, G. UAV-Based Evaluation of Rockfall Hazard in the Cultural Heritage Area of Kipinas Monastery, Greece. *Appl. Sci.* **2021**, *11*, 8946. [[CrossRef](#)]
34. Fanos, A.M.; Pradhan, B.; Mansor, S.; Yusoff, Z.M.; Abdullah, A.F.b. A hybrid model using machine learning methods and GIS for potential rockfall source identification from airborne laser scanning data. *Landslides* **2018**, *15*, 1833–1850. [[CrossRef](#)]
35. Li, H.-b.; Li, X.-w.; Li, W.-z.; Zhang, S.-l.; Zhou, J.-w. Quantitative assessment for the rockfall hazard in a post-earthquake high rock slope using terrestrial laser scanning. *Eng. Geol.* **2019**, *248*, 1–13. [[CrossRef](#)]
36. Konsolaki, A.; Vassilakis, E. Karst Topography Analysis Based on Multi-sensor (UAS & LiDAR) Data Acquisition. In Proceedings of the EGU2020, Vienna, Austria, 4–8 May 2020.
37. Vassilakis, E.; Konsolaki, A. Quantification of cave geomorphological characteristics based on multi source point cloud data interoperability. *Z. Fur Geomorphol.* **2022**, *63*, 265–277. [[CrossRef](#)]

38. Vassilakis, E.; Konsolaki, A.; Petrakis, S.; Kotsi, E.; Fillis, C.; Triantaphyllou, M.; Antonarakou, A.; Lekkas, E. Combination of close-range remote sensing data (TLS and UAS) and techniques for structural measurements across the deformation zone of the Ionian thrust in Zakynthos Isl. In Proceedings of the 16th International Congress of the Geological Society of Greece, Patras, Greece, 17–19 October 2022.
39. Konsolaki, A.; Vassilakis, E.; Karantanellis, E.; Asimakopoulou, K.; Lekkas, E.; Kotsi, E. Using multi-temporal digital twins of Navagio beach (Zakynthos Island, Greece) for the detection of rock displacements after the 8.9.2022 earthquake. In Proceedings of the 6th World Landslide Forum, Florence, Italy, 14–17 November 2023; p. 845.
40. Sarro, R.; Riquelme, A.; García-Davalillo, C.J.; Mateos, M.R.; Tomás, R.; Pastor, L.J.; Cano, M.; Herrera, G. Rockfall Simulation Based on UAV Photogrammetry Data Obtained during an Emergency Declaration: Application at a Cultural Heritage Site. *Remote Sens.* **2018**, *10*, 1923. [[CrossRef](#)]
41. Costanzo, D.; Rotigliano, E.; Irigaray, C.; Jiménez-Perálvarez, J.D.; Chacón, J. Factors selection in landslide susceptibility modelling on large scale following the gis matrix method: Application to the river Beiro basin (Spain). *Nat. Hazards Earth Syst. Sci.* **2012**, *12*, 327–340. [[CrossRef](#)]
42. Taymaz, T.; Jackson, J.; McKenzie, D. Active tectonics of the north and central Aegean Sea. *Geophys. Journal Int.* **1991**, *106*, 433–490. [[CrossRef](#)]
43. Nastos, P.T.; Karavana Papadimou, K.; Matsangouras, I.T. Mediterranean tropical-like cyclones: Impacts and composite daily means and anomalies of synoptic patterns. *Atmos. Res.* **2018**, *208*, 156–166. [[CrossRef](#)]
44. Diakakis, M.; Mavroulis, S.; Filis, C.; Lozios, S.; Vassilakis, E.; Naoum, G.; Soukis, K.; Konsolaki, A.; Kotsi, E.; Theodorakidou, D.; et al. Impacts of Medicanes on Geomorphology and Infrastructure in the Eastern Mediterranean, the Case of Medicane Ianos and the Ionian Islands in Western Greece. *Water* **2023**, *15*, 1026. [[CrossRef](#)]
45. Zafeiropoulos, G.; Drinia, H. Kalymnos Island, SE Aegean Sea: From Fishing Sponges and Rock Climbing to Geotourism Perspective. *Heritage* **2021**, *4*, 3126–3146. [[CrossRef](#)]
46. Papanikolaou, D.; Ebner, F. Tectono-stratigraphic maps and terrane descriptions. *Ann. Geol. Pays Hell.* **1997**, *37*, 195–197.
47. Papanikolaou, D. Tectonostratigraphic models of the Alpine terranes and subduction history of the Hellenides. *Tectonophysics* **2013**, *595–596*, 1–24. [[CrossRef](#)]
48. Grasmann, B.; Schneider, D.A.; Soukis, K.; Roche, V.; Hubmann, B. Paleogeographic position of the central Dodecanese Islands, southeastern Greece: The push-pull of Pelagonia. *GSA Bull.* **2022**, *134*, 1506–1528. [[CrossRef](#)]
49. Chatziioannou, E.; Grasmann, B.; Schneider, D.; Hubmann, B.; Soukis, K. Variscan tectonics in Dodecanese, Kalymnos island, Greece. In Proceedings of the EGU General Assembly Conference Abstracts, Vienna, Austria, 1 April 2015; p. 8409.
50. Triantafyllis, E.; Karfakis, I. The geological and tectonic structure of Kalymnos island (Dodecanese). *Bull. Geol. Soc. Greece* **1994**, 123–134.
51. Glade, T. Landslide occurrence as a response to land use change: A review of evidence from New Zealand. *CATENA* **2003**, *51*, 297–314. [[CrossRef](#)]
52. Reichenbach, P.; Busca, C.; Mondini, A.C.; Rossi, M. The Influence of Land Use Change on Landslide Susceptibility Zonation: The Briga Catchment Test Site (Messina, Italy). *Environ. Manag.* **2014**, *54*, 1372–1384. [[CrossRef](#)] [[PubMed](#)]
53. Achour, Y.; Boumezbeur, A.; Hadji, R.; Chouabbi, A.; Cavaleiro, V.; Bendaoud, E.A. Landslide susceptibility mapping using analytic hierarchy process and information value methods along a highway road section in Constantine, Algeria. *Arab. J. Geosci.* **2017**, *10*, 194. [[CrossRef](#)]
54. Zhao, P.; Masoumi, Z.; Kalantari, M.; Aflaki, M.; Mansourian, A. A GIS-Based Landslide Susceptibility Mapping and Variable Importance Analysis Using Artificial Intelligent Training-Based Methods. *Remote Sens.* **2022**, *14*, 211. [[CrossRef](#)]
55. Ilia, I.; Tsangaratos, P. Applying weight of evidence method and sensitivity analysis to produce a landslide susceptibility map. *Landslides* **2016**, *13*, 379–397. [[CrossRef](#)]
56. Mavroulis, S.; Diakakis, M.; Kranis, H.; Vassilakis, E.; Kapetanidis, V.; Spingos, I.; Kaviris, G.; Skourtsos, E.; Voulgaris, N.; Lekkas, E. Inventory of Historical and Recent Earthquake-Triggered Landslides and Assessment of Related Susceptibility by GIS-Based Analytic Hierarchy Process: The Case of Cephalonia (Ionian Islands, Western Greece). *Appl. Sci.* **2022**, *12*, 2895. [[CrossRef](#)]
57. Psomiadis, E.; Charizopoulos, N.; Efthimiou, N.; Soulis, K.X.; Charalampopoulos, I. Earth Observation and GIS-Based Analysis for Landslide Susceptibility and Risk Assessment. *ISPRS Int. J. Geo-Inf.* **2020**, *9*, 552. [[CrossRef](#)]
58. Saaty, R.W. The analytic hierarchy process—What it is and how it is used. *Math. Model.* **1987**, *9*, 161–176. [[CrossRef](#)]
59. Goepel, K.D. Implementation of an Online Software Tool for the Analytic Hierarchy Process (AHP-OS). *Int. J. Anal. Hierarchy Process* **2018**, *10*, 469–487. [[CrossRef](#)]
60. Kotsi, E.; Vassilakis, E.; Diakakis, M.; Mavroulis, S.; Konsolaki, A.; Filis, C.; Lozios, S.; Lekkas, E. Using UAS-Aided Photogrammetry to Monitor and Quantify the Geomorphic Effects of Extreme Weather Events in Tectonically Active Mass Waste-Prone Areas: The Case of Medicane Ianos. *Appl. Sci.* **2023**, *13*, 812. [[CrossRef](#)]
61. Panagiotopoulou, S.; Erkeki, A.; Antonakakis, A.; Grigorakakis, P.; Protopapa, V.; Tsiostas, G.; Vlachou, K.; Vassilakis, E. Evaluation of Network Real Time Kinematics contribution to the accuracy/productivity ratio for UAS-SfM Photogrammetry. In Proceedings of the 2020 European Navigation Conference (ENC), Dresden, Germany, 23–24 November 2020; pp. 1–11.

-
62. Agisoft. *Metashape Professional*, 2.0.2 build 16404; Agisoft LLC: St. Petersburg, Russia, 2023.
 63. RocScience. *RocFall2*, 8.024; Rocscience Inc.: Toronto, ON, Canada, 2023.

Disclaimer/Publisher's Note: The statements, opinions and data contained in all publications are solely those of the individual author(s) and contributor(s) and not of MDPI and/or the editor(s). MDPI and/or the editor(s) disclaim responsibility for any injury to people or property resulting from any ideas, methods, instructions or products referred to in the content.